

1 **Monitoring high-ozone events in the US Intermountain West using TEMPO**
2 **geostationary satellite observations**

3

4 Peter Zoogman^{1, †, *}, Daniel J. Jacob^{1,2}, Kelly Chance³, Xiong Liu³, Meiyun Lin⁴, Arlene Fiore⁵,
5 Katherine Travis²

6

7 1 Department of Earth and Planetary Sciences, Harvard University, Cambridge, MA, United
8 States

9 2 School of Engineering and Applied Sciences, Harvard University, Cambridge, MA, United
10 States

11 3 Harvard-Smithsonian Center for Astrophysics, Cambridge, MA, United States

12 4 Atmospheric and Ocean Sciences, Princeton University, Princeton, New Jersey, USA

13 5 Lamont-Doherty Earth Observatory, Columbia University, Palisades, NY, United States

14 † Present Address: Harvard-Smithsonian Center for Astrophysics, Cambridge, MA, United
15 States

16 *Corresponding Author. Tel: 9176129834. E-mail: pzoogman@cfa.harvard.edu. 60 Garden
17 Street, Cambridge, MA 02138

18 **Abstract**

19 High-ozone events, approaching or exceeding the National Ambient Air Quality Standard
20 (NAAQS), are frequently observed in the US Intermountain West in association with subsiding
21 air from the free troposphere. Monitoring and attribution of these events is problematic because
22 of the sparsity of the current network of surface measurements and lack of vertical information.
23 We present an Observing System Simulation Experiment (OSSE) to evaluate the ability of the
24 future geostationary satellite instrument Tropospheric Emissions: Monitoring of Pollution
25 (TEMPO), scheduled for launch in 2018-2019, to monitor and attribute high-ozone events in the
26 Intermountain West through data assimilation. TEMPO will observe ozone in the ultraviolet
27 (UV) and visible (Vis) to provide sensitivity in the lower troposphere. Our OSSE uses ozone data
28 from the GFDL AM3 chemistry-climate model (CCM) as the “true” atmosphere and samples it
29 for April-June 2010 with the current surface network (CASTNet sites), TEMPO, and a low Earth
30 orbit (LEO) IR satellite instrument. These synthetic data are then assimilated into the GEOS-
31 Chem chemical transport model (CTM) using a Kalman filter. Error correlation length scales
32 (500 km in horizontal, 1.7 km in vertical) extend the range of influence of observations. We
33 show that assimilation of surface data alone does not adequately detect high-ozone events in the
34 Intermountain West. Assimilation of TEMPO data greatly improves the monitoring capability,
35 with little information added from the LEO instrument. The vertical information from TEMPO
36 further enables the attribution of NAAQS exceedances to background ozone. This is illustrated
37 with the case of a stratospheric intrusion.

38

39 **1. Introduction**

40 Harmful impacts of surface level ozone on both humans and vegetation is of increasing
41 concern in areas formerly considered remote. The US Environmental Protection Agency (EPA) is
42 considering lowering the current National Ambient Air Quality Standard (NAAQS) of 75 ppbv (fourth
43 highest maximum daily 8-hour average per year) to a value in the range of 60-70 ppbv (EPA, 2012).
44 Ozone concentrations in this range are frequently observed at high-elevation sites in the western US
45 with minimal local pollution influence (Lefohn et al., 2001). Although ozone levels have been
46 decreasing over the eastern US for the past two decades due to emissions controls, there has been no
47 such decrease in the West except for California (Cooper et al., 2012). Free tropospheric ozone at
48 3-8 km altitude over the western US has been increasing by 0.41 ppbv year⁻¹ during the past two
49 decades (Cooper et al., 2012), which could affect background surface concentrations in the West
50 (Zhang et al., 2008). There has been great interest in using satellite observations of ozone and
51 related species to monitor and attribute background surface ozone (Lin et al., 2012a; Fu et al.,
52 2013). This capability has been limited so far by the temporal sparseness of satellite data and low
53 sensitivity to the surface. All satellite measurements so far have been from low Earth orbit
54 (LEO). Here we show that multispectral measurements from the NASA Tropospheric Emissions:
55 Monitoring of Pollution (TEMPO) geostationary satellite mission over North America, scheduled
56 for launch in 2018-2019, can provide a powerful ozone monitoring resource to complement
57 surface sites, and can help to identify NAAQS exceedances caused by elevated background.

58 The North American background is defined by the EPA as the surface ozone concentration
59 that would be present over the US in the absence of North American anthropogenic emissions. It
60 includes natural sources and intercontinental pollution, and represents a floor for the achievable
61 benefits from domestic emissions control policies (including agreements with Canada and

62 Mexico). The North American background is particularly high in the Intermountain West, a
63 region extending between the Sierra Nevada/Cascades on the west and the Rocky Mountains on
64 the east, due to high elevation and arid terrain (Zhang et al., 2011). Subsidence of high-ozone air
65 from the free troposphere can cause surface ozone concentrations in that region to approach or exceed
66 the NAAQS (Reid et al., 2008). This is not an issue in the eastern US because of lower elevation,
67 forest cover, and high moisture (Fiore et al., 2002).

68 Background effects on surface ozone air quality are important to diagnose, as NAAQS
69 exceedances can be dismissed as exceptional events if shown to be not reasonably controllable
70 by local governances (EPA 2013). Monitoring of ozone in the Intermountain West is mostly
71 performed at urban stations designed to observe local pollution and not background influences.
72 There is a limited network of Clean Air Status and Trends Network (CASTNet;
73 www.epa.gov/castnet) sites located at national parks and other remote locations, and these have
74 been used extensively to estimate background ozone and evaluate models (Fiore et al., 2002;
75 Zhang et al., 2011; Lin et al., 2012b; Cooper et al., 2012). Langford et al. (2009) demonstrated
76 that transport of stratospheric air contributed to surface one-minute average ozone concentrations
77 in excess of 100 ppbv in Colorado in 1999. Analysis of ozonesonde and lidar measurements by
78 Lin et al [2012b] indicates thirteen stratospheric intrusions in spring 2010 leading to observed
79 maximum daily 8-hour average (MDA8) ozone of 70-86 ppbv at surface sites. Yates et al. (2013)
80 similarly demonstrated a stratospheric origin for a NAAQS exceedance in Wyoming in June
81 2012 by using a combination of 3-D modeling, aircraft observations, LEO satellite data, and
82 geostationary weather satellites. But the current air quality observing system is very limited in
83 its ability to (1) monitor ozone at sites prone to high background, and (2) diagnose the origin of
84 high-ozone events at these sites.

85 Several chemical transport models (CTMs) and one chemistry-climate model (CCM)
86 have been used to estimate the North American background including GEOS-Chem (Fiore et al.,
87 2003; Zhang et al., 2011), GFDL AM3 CCM (Lin et al., 2012a,b), CMAQ (Mueller and Mallard
88 2011), and CAMx (Emery et al., 2012). Values average 30-50 ppbv in spring and summer over
89 the Intermountain West with events exceeding 60 ppbv. There are large differences between
90 models reflecting variable contributions from the stratosphere (Lin et al. 2012b), lightning
91 (Kaynak et al. 2008, Zhang et al. 2011), and wildfires (Mueller and Mallard, 2011; Zhang et al.,
92 2011; Jaffe and Wigder, 2012; Singh et al., 2012).

93 Geostationary satellites are a promising tool to address the limitations of the current observing
94 system (Fishman et al., 2012; Lahoz et al., 2012). These satellites orbit the Earth with a 24-h period in
95 an equatorial plane, thus continuously staring at the same scenes. Depending on the observing strategy,
96 they may provide hourly ozone data over a continental domain, while a LEO satellite may offer at best
97 a 1-day return time. A global constellation of geostationary satellite missions targeted at air quality is
98 planned to launch in 2018-2019 including TEMPO over North America (Chance et al. 2012),
99 SENTINEL-4 over Europe (Ingmann et al., 2012), and GEMS over East Asia (Kim 2012; Bak et al.,
100 2013).

101 TEMPO will measure backscattered solar radiation in the 290-740 nm range, including
102 the ultraviolet (UV) and visible Chappuis (Vis) ozone bands (Chance et al., 1997; Liu et al.,
103 2005). Sentinel-4 and GEMS will only measure ozone in the UV. Observation in the weak
104 Chappuis band takes advantage of the relative transparency of the atmosphere in the Vis to
105 achieve sensitivity to near-surface ozone (Natraj et al., 2011; Selitto et al., 2012a). An observing

106 system simulation experiment (OSSE) by Zoogman et al. (2011) shows that a UV+Vis instrument in
107 geostationary orbit could provide useful constraints on surface ozone through data assimilation.

108 Here we conduct an OSSE to quantify the potential of geostationary ozone measurements
109 from TEMPO to improve monitoring of ozone NAAQS exceedances in the Intermountain West
110 and the role of background ozone in causing these exceedances. Our goal is to inform the TEMPO
111 observing strategy and develop methods for exploitation of TEMPO data. OSSEs have previously
112 informed mission planning for geostationary observations of atmospheric composition (Edwards et al.,
113 2009; Timmermans et al., 2009; Zoogman et al., 2011, 2014, Claeys et al., 2011, Selitto et al.,
114 2014). An important feature of our work here is the inclusion of surface network and LEO
115 satellite observations in the data assimilation system to properly quantify the added benefit of
116 TEMPO observations.

117 Section 2 outlines the OSSE framework including a description and comparison of the
118 simulation models used, the present and future observing systems considered, the data
119 assimilation system, and the quantification of the error correlation length scales. Section 3
120 describes the OSSE results showing improved monitoring of surface ozone across the
121 Intermountain West from TEMPO observations and improved detection of high-ozone events in
122 the Intermountain West by data assimilation. Section 4 presents a case study of a stratospheric
123 intrusion demonstrating the detection of an exceptional ozone event by TEMPO its attribution to
124 the North American background. Section 5 summarizes the results and discusses future research
125 directions.

126 **2. Observing System Simulation Experiment (OSSE)**

127 OSSEs are a standard technique for assessing the information to be gained by data assimilation
128 from adding a new instrument to an existing observing system (Lord et al., 1997). The OSSE
129 framework involves the use of a model to generate synthetic time-varying 3-D fields of concentrations
130 (taken as the “true” atmosphere), and the virtual sampling of this “true” atmosphere by the different
131 instruments composing the observing system for data assimilation. This virtual sampling follows the
132 observing schedules and error characteristics of each instrument. The virtual observations are then
133 assimilated in a second, independent model, and the results of the assimilation (with and without the
134 new instrument) are compared to the “true” atmosphere to assess the value of the new instrument
135 (Edwards et al., 2009).

136 We conduct our OSSE for April-June 2010, corresponding to the seasonal maximum in
137 background ozone over the Intermountain West (Brodin et al., 2010). The observing system includes
138 the CASTNet surface network, a LEO instrument, and TEMPO. The “true” atmosphere is provided by
139 the GFDL AM3 CCM (Lin et al., 2012a,b). The model used for data assimilation (“forward model”) is
140 the GEOS-Chem CTM (Zhang et al, 2011); it generates *a priori* concentrations at successive time steps
141 to be corrected to the “true” atmosphere by the observing system through data assimilation. The
142 information provided by the observing system is quantified by the correction of the mismatch between
143 the “true” state and the *a priori*. We describe below our OSSE framework including the simulation
144 models (GFDL AM3 and GEOS-Chem), the observing system, and the data assimilation system.

145 **2.1 Simulation Models**

146 We use for our “true” atmosphere the GFDL AM3 global chemistry-climate model with
147 horizontal resolution of $1/2^\circ \times 5/8^\circ$ (latitude x longitude) nudged to reanalysis winds (Lin et al.,
148 2012a,b). This CCM was successful in reproducing background ozone variability and exceptional
149 events in the Western US during the CalNex field campaign in April-June 2010 (Lin et al., 2012b).
150 This is important because the “true” model should reproduce the characteristics of the
151 observations relevant to the OSSE. Lin et al. (2012a,b) used GFDL AM3 to investigate the effect of
152 Asian transport and stratospheric intrusions on surface ozone in the Intermountain West during April-
153 June 2010, and they quantified the ozone background through a sensitivity simulation with North
154 American anthropogenic sources shut off. Here we use 3-hourly concentrations archived from
155 their standard simulation to provide the global 3-D ozone fields of the “true” atmosphere.

156 Our forward model for data assimilation is the GEOS-Chem CTM (Bey et al., 2001;
157 <http://www.geos-chem.org>) driven by GEOS assimilated meteorological data from the NASA Global
158 Modeling and Assimilation Office (GMAO). The GEOS-Chem version used here (v8-02-03) was
159 previously described by Zhang et al. (2011) in a study of background ozone influence on the
160 Intermountain West during 2006-2008. It covers the North America domain with $1/2^\circ \times 2/3^\circ$
161 horizontal resolution ($10^\circ\text{N} - 60^\circ\text{N}$, $140^\circ\text{W} - 40^\circ\text{W}$), nested within a global domain with $2^\circ \times 2.5^\circ$
162 horizontal resolution. GEOS-Chem and GFDL AM3 have completely separate development heritages
163 and use different driving meteorological fields, chemical mechanisms, and emission inventories. This
164 independence between the two models used in the OSSE is important for a rigorous assessment
165 (Arnold and Dey 1986). The horizontal resolution of both models (~50 km) is adequate for
166 characterization of background ozone.

167 **Figure 1** shows the maximum daily average 8-hour (MDA8) ozone concentrations in surface
168 air for each model, averaged over April-June 2010. GFDL AM3 has higher ozone concentrations than
169 GEOS-Chem over the US as a whole and over the Intermountain West (bordered region) in particular.
170 Zhang et al. (2011) previously showed that GEOS-Chem can reproduce ozone concentrations in
171 the Intermountain West up to 70 ppbv with relatively little error, but cannot reproduce
172 exceptional events of higher concentrations. GFDL AM3 is biased high in the mean but better
173 simulates high-ozone events (Lin et al., 2012b).

174

175 2.2 Observing System and Synthetic Observations

176 Our OSSE simulates the anticipated ozone observing system over the Intermountain West
177 during operation of TEMPO. This will consist of surface measurements, LEO satellite
178 measurements, and TEMPO geostationary satellite measurements. For the LEO satellite
179 measurements we assume a future version of the Infrared Atmospheric Sounding Interferometer
180 (IASI) instrument, IASI-3, that will be launched in 2016 on the MetOp-C satellite (Clerbaux, 2009).
181 IASI retrieves ozone in the thermal infrared (TIR). We also expect to have in that time frame UV ozone
182 observations from the TROPOspheric Monitoring Instrument (TROPOMI), scheduled for LEO
183 launch in 2015 (<http://www.tropomi.eu>). TIR and UV ozone instruments have similar vertical
184 sensitivities (Zhang et al., 2010). TIR has the advantage of providing observations at night that will be
185 complementary to TEMPO.

186 CASTNet provides hourly data for 12 surface sites in the Intermountain West (Figure 1)
187 that are used for background monitoring (EPA, 2013). Although these sites are sparse, they are
188 intended to be regionally representative and exhibit significant spatial correlation (Jaffe, 2011).
189 CASTNet stations outside of the Intermountain West are not used; we assumed they do not

190 provide useful constraints for the region but it is possible certain California sites might be
191 exceptions. CASTNet ozone measurements have 2% instrument error (EPA, 2010). There is
192 additional representation error when assimilating CASTNet data into a model due to the spatial
193 mismatch between the point where the measurement is taken and the model gridsquare mean to
194 which it is compared. We find a representation error of 5% for the $\sim 50 \times 50 \text{ km}^2$ gridsquare size of
195 GEOS-Chem, based on the model error correlation length scale (see Section 2.4). During
196 nighttime the representation error could be much larger due to surface air stratification. Thus we
197 only assimilate CASTNet data during daytime.

198 TEMPO and IASI-3 are both nadir viewing satellite instruments, with retrieval of vertical
199 concentration profiles to be made by optimal estimation (Rodgers, 2000). If \mathbf{x}_p is the true profile,
200 i.e. the vector of true concentrations in an observation column, then the retrieved profile \mathbf{x}_p' is
201 related to \mathbf{x}_p by the instrument averaging kernel matrix \mathbf{A} which defines the sensitivity of \mathbf{x}_p' to
202 \mathbf{x}_p ($\mathbf{A} = \partial \mathbf{x}_p' / \partial \mathbf{x}_p$):

$$203 \quad \mathbf{x}_p' = \mathbf{x}_s + \mathbf{A}(\mathbf{x}_p - \mathbf{x}_s) + \boldsymbol{\varepsilon} \quad (1)$$

204 where $\boldsymbol{\varepsilon}$ is the instrument noise vector and \mathbf{x}_s is an independent *a priori* ozone profile used to
205 regularize the retrieval.

206 **Figure 2** shows typical clear-sky averaging kernel matrices for UV+Vis and TIR retrievals of
207 tropospheric ozone taken from the Natraj et al. (2011) theoretical study. Also shown are the degrees
208 of freedom for signal (DOFS) below given pressure levels. The DOFS are the number of independent
209 pieces of information in the vertical provided by the retrieval, as determined from the corresponding
210 trace of the averaging kernel matrix. The profile (index 5 from Natraj et al. 2011) used to generate
211 these averaging kernels has moderate ozone (58 ppbv), moderate temperature contrast, and an
212 intermediate viewing geometry, making it consistent with conditions in the Intermountain West.
213 The assumed Vis surface albedo may be lower than the actual albedo which would result in an
214 underestimation of TEMPO sensitivity to near-surface ozone. The UV+Vis spectral ranges (290-
215 340 nm, 560-620 nm) and spectral resolution (0.4 nm) assumed by Natraj et al. (2011) are
216 comparable to the spectral ranges (290-490 nm, 540-740 nm) and spectral resolution (0.6 nm)
217 planned for TEMPO. The TEMPO instrument is still under development and thus does not have
218 its characteristics fully finalized; Natraj et al. (2011) gives the published best estimate of
219 TEMPO ozone sensitivities. We expect TEMPO ozone sensitivities to be similar to UV+Vis
220 sensitivities from Natraj et al. (2011). The additional near-surface information provided by the
221 UV+Vis combination is consistent with previous work using SCIAMACHY data (Selitto et al.,
222 2012b).

223 We generate synthetic TEMPO geostationary observations from the GFDL AM3 “true”
224 atmosphere by sampling daytime vertical profiles over land in the North American domain with the
225 averaging kernel matrix given in **Figure 2**. TEMPO observations over the ocean are not included as the
226 planned field of regard for the mission includes very little ocean and because the clear ocean surface is
227 too dark for Vis retrievals. We similarly generate synthetic LEO IASI-3 (henceforth LEO) observations
228 over the North American domain twice a day (local noon and midnight) with the averaging kernel
229 matrix given in **Figure 2**. These TIR measurements are intended as representative of ozone
230 observations from LEO instruments operational during the TEMPO lifetime. We omit scenes with
231 cloud fraction > 0.3 (as given by the GEOS meteorological data). We assume fixed averaging kernel
232 matrices, acknowledging that in practice there is significant variability (Worden et al., 2013).

233 Gaussian noise is added to the synthetic observations following Natraj et al. (2011) to simulate the
 234 random error associated with the spectral measurement. The noise from the TEMPO instrument
 235 (footprint of 4x8 km²) is reduced by the square root of the number of observations averaged over each
 236 GEOS-Chem grid square (~50x50 km²) in the data assimilation process. Since the TEMPO
 237 measurements are spatially dense we assume zero representation error during assimilation. Current
 238 IASI measurements have footprint diameters of 12-40 km with centers spaced 25-80 km apart (August
 239 et al., 2012); no reduction of the random error is applied to the LEO observations.

240 2.3 Assimilation of surface and satellite measurements

241 The goal of our data assimilation system is to optimize an n -element state vector (\mathbf{x}) of 3-
 242 D tropospheric ozone concentrations over the North American domain of GEOS-Chem, using
 243 surface and satellite observations to correct the GEOS-Chem simulation at successive time steps.
 244 CASTNet and TEMPO data are assimilated at discrete 3-h time steps, and LEO data are
 245 assimilated at 12-h time steps. We use a Kalman filter, as previously applied to ozone data
 246 assimilation by Khatatov et al (2000), Parrington et al. (2008), and Zoogman et al. (2011). At
 247 each time step, we calculate an optimal estimate $\hat{\mathbf{x}}$ of the true ozone concentrations \mathbf{x} as a weighted
 248 average of the model forecast \mathbf{x}_a (with corresponding error vector $\boldsymbol{\varepsilon}_a$ relative to the true concentrations)
 249 and the observations \mathbf{x}' (with observational error $\boldsymbol{\varepsilon}'$ and with \mathbf{x}' set to \mathbf{x}_a where there are no
 250 observations). The observational error includes both the instrument noise $\boldsymbol{\varepsilon}$ and (for surface sites) the
 251 previously defined representation error. The errors are characterized by error covariance matrices $\mathbf{S}_a =$
 252 $E[\boldsymbol{\varepsilon}_a \boldsymbol{\varepsilon}_a^T]$ and $\mathbf{S}_\varepsilon = E[\boldsymbol{\varepsilon}' \boldsymbol{\varepsilon}'^T]$, where $E[\]$ is the expected-value operator. Assuming Gaussian error
 253 distributions for $\boldsymbol{\varepsilon}_a$ and $\boldsymbol{\varepsilon}$ we obtain (Rodgers, 2000):

$$254 \quad \hat{\mathbf{x}} = \mathbf{x}_a + \mathbf{G}(\mathbf{x}' - \mathbf{K}\mathbf{x}_a) \quad (2)$$

255 where \mathbf{K} is the observation operator that maps the model forecast to the observations. For satellite
 256 measurements $\mathbf{K}\mathbf{x}_a = \mathbf{x}_s + \mathbf{A}(\mathbf{x}_a - \mathbf{x}_s)$ (equation (1) with no noise term), while for surface measurements
 257 $\mathbf{K}\mathbf{x}_a = \mathbf{x}_a$. The gain matrix \mathbf{G} is given by

$$258 \quad \mathbf{G} = \mathbf{S}_a \mathbf{K}^T (\mathbf{K} \mathbf{S}_a \mathbf{K}^T + \mathbf{S}_\varepsilon)^{-1} \quad (3)$$

259 and determines the relative weight given to the observations and the model. The instrument error
 260 covariance matrix \mathbf{S}_ε is assumed diagonal and set to an arbitrarily large number in locations
 261 where there are no observations. For surface measurements we include the 5% representation
 262 error in quadrature with the 2% instrument error so that the corresponding error variances are
 263 additive. The optimal estimate $\hat{\mathbf{x}}$ has error $\hat{\boldsymbol{\varepsilon}}$ with error covariance $\hat{\mathbf{S}} = E[\hat{\boldsymbol{\varepsilon}} \hat{\boldsymbol{\varepsilon}}^T]$:

$$264 \quad \hat{\mathbf{S}} = (\mathbf{I}_n - \mathbf{G}\mathbf{K})\mathbf{S}_a \quad (4)$$

265 Where \mathbf{I}_n is the identity matrix of dimension n .

266 The model error covariance matrix \mathbf{S}_a expresses the error in the forward model at each
 267 assimilation time step and is given by:

268

$$\mathbf{S}_a = \begin{pmatrix} \text{var}(\boldsymbol{\varepsilon}_{a,1}) & \cdots & \text{cov}(\boldsymbol{\varepsilon}_{a,1}, \boldsymbol{\varepsilon}_{a,n}) \\ \vdots & \ddots & \vdots \\ \text{cov}(\boldsymbol{\varepsilon}_{a,n}, \boldsymbol{\varepsilon}_{a,1}) & \cdots & \text{var}(\boldsymbol{\varepsilon}_{a,n}) \end{pmatrix} \quad (5)$$

269 where $\boldsymbol{\varepsilon}_a = (\boldsymbol{\varepsilon}_{a,1}, \dots, \boldsymbol{\varepsilon}_{a,n})^T$, with $\boldsymbol{\varepsilon}_{a,i}$ representing the error for GEOS-Chem gridbox i . Following
 270 Zoogman et al. (2011), we initialize \mathbf{S}_a at the beginning of the simulation as a diagonal matrix
 271 with *a priori* errors of 29%, and update it at each assimilation time step on the basis of the
 272 computed *a posteriori* error covariance matrix $\hat{\mathbf{S}}$ (equation (4)). The diagonal terms of $\hat{\mathbf{S}}$ are
 273 transported as tracers in GEOS-Chem to the next assimilation time step and are augmented by a model
 274 error variance reflecting the time-dependent divergence of the model from the true state (Zoogman et
 275 al., 2011). This yields the diagonal terms $\text{var}(\boldsymbol{\varepsilon}_{a,i})$ of \mathbf{S}_a for the next assimilation time step. The
 276 off-diagonal terms (error covariances) describe the propagation of information from each
 277 observation over a spatial domain of influence. We compute $\text{cov}(\boldsymbol{\varepsilon}_{a,i}, \boldsymbol{\varepsilon}_{a,j})$ for each pair of
 278 gridboxes (i,j) as a function of the horizontal and vertical distance between the two gridboxes
 279 using the error correlation length scales from section 2.4.

280 In practice the dimension of the matrices used in the assimilation must be limited to make
 281 the computation tractable. This is done by solving (2) column by column and including only
 282 measurements at a horizontal distance less than 510 km (the horizontal error correlation length
 283 scale, see below) in the model error covariance matrix.

284

285 2.4 Error Correlation Length Scales

286 The spatial extent of information provided by an observation to correct the GEOS-Chem
 287 model simulation through data assimilation can be quantified by correlating the GEOS-Chem
 288 errors relative to *in situ* observations at different sites in the Intermountain West (for the
 289 horizontal scale) and ozonesonde profiles (for the vertical scale). To define a horizontal error
 290 correlation length scale we used actual CASTNet surface measurements from our period of study
 291 (April-June 2010), downloaded from <http://epa.gov/castnet/>. We compute the time series of
 292 model error during daytime (0900 – 1700 LT) at each surface site, and from there derive the
 293 model error correlation between each pair of surface sites. **Figure 3 (left)** shows the correlation
 294 coefficients plotted against the distance d between sites (binned every 100km). We find $R = \exp(-$
 295 $d/510 \text{ km})$. We also show the error correlation length scale calculated when comparing GEOS-
 296 Chem and GFDL AM3 (in red) sampled over the Intermountain West region. The model-model
 297 error correlation length scale is similar to the model-observation length scale, providing support
 298 for the realism of error patterns in our OSSE. We assume that the horizontal error correlation
 299 length scale is invariant with altitude.

300 To estimate the vertical correlation length scale we compare GEOS-Chem ozone
 301 concentrations to *in situ* vertical profiles from May-June 2010 ozonesondes at six locations in
 302 California (Cooper et al. 2011). **Figure 3 (right)** shows the correlation coefficients plotted
 303 against the vertical distance z (binned every 500 m) for the time series of model errors at each
 304 ozonesonde station from the surface to 8 km altitude. We find $R = \exp(-z/1.7 \text{ km})$. Again, the
 305 model-model length scale (red) is not significantly different from the model-observation length
 306 scale.

307

308 3. TEMPO observation of high-ozone events in the Intermountain West

309 We now apply our OSSE system to evaluate the benefit of TEMPO observations to
310 monitor and attribute ozone exceedances in the Intermountain West. We compare the “true”
311 concentrations in surface air over the Intermountain West to GEOS-Chem CTM ozone
312 concentrations without data assimilation (*a priori*) and with assimilation of synthetic CASTNet,
313 TEMPO, and IASI-3 LEO observations. We also performed an assimilation of CASTNet and
314 TEMPO observations without a LEO instrument and found no significant difference in results.
315 Thus the LEO instrument does not add significant information beyond TEMPO for constraining
316 surface ozone concentrations in the Intermountain West. Its value for tracking exceptional events
317 will be discussed in section 4.

318 **Figure 4** examines the ability of the data assimilation system to monitor daily MDA8
319 ozone over the Intermountain West at the $1/2^\circ \times 2/3^\circ$ ($\sim 50 \times 50 \text{ km}^2$) GEOS-Chem grid resolution.
320 The top panel shows a scatterplot of *a priori* GEOS-Chem MDA8 ozone concentrations in April-
321 June 2010, for individual grid squares over the Intermountain West domain of Figure 1 and
322 individual days, vs. the “true” concentrations from the GFDL AM3 model. The GEOS-Chem *a*
323 *priori* is biased low and performs poorly in reproducing the “true” variability ($R^2=0.12$, bias = -
324 9.0 ppbv). Assimilation of synthetic CASTNet surface measurements reduces the low bias from
325 9.0 to 2.8 ppbv, but still does not capture much of the variability ($R^2=0.34$). Adding the synthetic
326 TEMPO geostationary observations eliminates the low bias and captures over half of the
327 variability ($R^2=0.58$).

328 The ability of TEMPO observations to capture high-ozone events is of particular interest.
329 **Figure 5** shows a map of the number of days in April-June 2010 with MDA8 ozone in excess of
330 70 ppbv for individual GEOS-Chem gridsquares in the Intermountain West. Values are shown
331 for the “true” atmosphere, the GEOS-Chem *a priori* without data assimilation, and the data
332 assimilation results including only the CASTNet observations and with the addition of TEMPO
333 observations. The “truth” shows an average of 5.7 high-ozone events per gridsquare in the
334 Intermountain West over the April-June 2010 period. The *a priori* model has only 0.8 event-days
335 per gridsquare and the spatial pattern is very different (spatial correlation $R^2=0.09$ for the
336 ensemble of Intermountain West gridsquares). Assimilation of surface measurements improves
337 both the average number of high-ozone events (3.6 event-days) and the spatial pattern ($R^2=0.62$).
338 The inability to fully correct the bias is due in part to the large impact of free tropospheric air in
339 driving high-ozone events, and in part to the limited coverage from the sparse surface network.
340 Adding TEMPO satellite observations almost fully corrects the bias (mean of 5.4 event-days)
341 and captures most of the spatial distribution of high-ozone events ($R^2=0.82$).

342

343 4. Attribution of exceptional events using TEMPO observations

344 TEMPO will provide continuous daytime observation in the free troposphere as well as in
345 the boundary layer, with separation between the two (Figure 2). Thus it could be particularly
346 powerful in quantifying free tropospheric background contributions to NAAQS exceedances.
347 This would assist in the designation of exceptional events where an exceedance of the NAAQS is
348 considered to be outside local control.

349 We examine a case study of a stratospheric intrusion on June 13 in the GFDL AM3
350 model taken as the “truth”. **Figure 6** shows a time series for June 2010 of MDA8 ozone
351 concentrations at a location in northern New Mexico (107°W , 36°N). We choose this event as it

352 was diagnosed by ozonesonde observations and meteorological tracers as a deep stratospheric
353 intrusion event (Lin et al., 2012a). Actual observations at nearby CASTNet locations indicate
354 ozone in excess of 75 ppbv during this modeled intrusion.

355 Evidence of free tropospheric origin for the June 13 event is critical to achieving an
356 “exceptional event” designation. **Figure 7** (top left) shows a longitude-altitude cross section of
357 ozone concentrations in the GFDL AM3 model taken as the “truth”. The stratospheric intrusion
358 is manifest at 103-109°W. The *a priori* GEOS-Chem model (top right) also shows a stratospheric
359 ozone enhancement extending to the surface but of much smaller magnitude. Assimilation of
360 surface measurements (not shown) makes little correction in the free troposphere. Synthetic
361 satellite measurement imagery from TEMPO without assimilation (bottom left) shows elevated
362 values in the free troposphere but does not properly represent surface gradients due to instrument
363 smoothing. Assimilating TEMPO observations into the GEOS-Chem CTM together with LEO
364 measurements (bottom right) captures the magnitude and spatial structure of the stratospheric
365 intrusion, and this would make a strong case for diagnosis of an exceptional event. We see here
366 that the use of data assimilation efficiently enhances the information from TEMPO to constrain
367 surface air concentrations. Information from the LEO instrument does not add significantly in
368 this case to observations from TEMPO, although it does correct ozone fields over the ocean
369 where TEMPO does not observe in this OSSE. The LEO instrument will thus be valuable for
370 tracking transpacific transport of ozone plumes even when TEMPO is operational.

371

372 **5. Summary**

373 We demonstrated the potential of future TEMPO UV+Vis geostationary observations to
374 monitor ozone exceedances in the Intermountain West and identify those exceedances caused by
375 the North American background. Our goal was to inform the TEMPO observing strategy and
376 develop methods for exploitation of its data. To accomplish this we performed an observation system
377 simulation experiment (OSSE) for assimilation of the TEMPO data using two global 3-D ozone
378 models with ~50 km horizontal resolution, one as the “true” atmosphere and one as the forward model
379 for data assimilation. We also included in our OSSE surface measurements from the current CASTNet
380 monitoring network sites in the Intermountain West (12 sites) and satellite measurements from a
381 thermal infrared (TIR) low Earth orbit (LEO) instrument projected to be in orbit concurrently with
382 TEMPO.

383 An important factor in data assimilation is the scales over which observed information
384 can be propagated with the forward model. We quantified this using model error correlation
385 length scales for the Intermountain West based on actual CASTNet and ozonesonde data. We
386 find length scales of 500 km (horizontal) and 1.7 km (vertical). These are in close agreement
387 with error correlation length scales between the two models used in our OSSE.

388 We find that the CASTNet surface observations are too sparse to adequately monitor
389 high-ozone events in the Intermountain West even after data assimilation. We show that the
390 TEMPO geostationary observations will provide a greatly improved observing system for
391 monitoring such events, eliminating the *a priori* model bias, capturing 58% of surface MDA8
392 ozone variability, and capturing 82% of the distribution of high-ozone days. In addition, because
393 of the information they provide on the vertical distribution of ozone, they can effectively
394 diagnose NAAQS exceedances caused by background ozone. A LEO satellite instrument flying
395 concurrently with TEMPO provide no significant added value for monitoring the ozone
396 background over the US but could be useful for tracking transpacific plumes.

397 The use of invariant averaging kernel matrices is a limitation of this study. Preparation
398 for TEMPO must include improved constraints on physical parameters, such as surface albedo,
399 that can vary greatly over the North American domain and that affect the sensitivity of UV+Vis
400 retrievals of near-surface ozone. Also, if the differences between the two models used in our
401 OSSE are larger than future errors in modeled ozone, this study may overestimate the
402 information TEMPO will provide. However, our OSSE demonstrates the large relative
403 improvement of information provided by TEMPO over the current observing system.

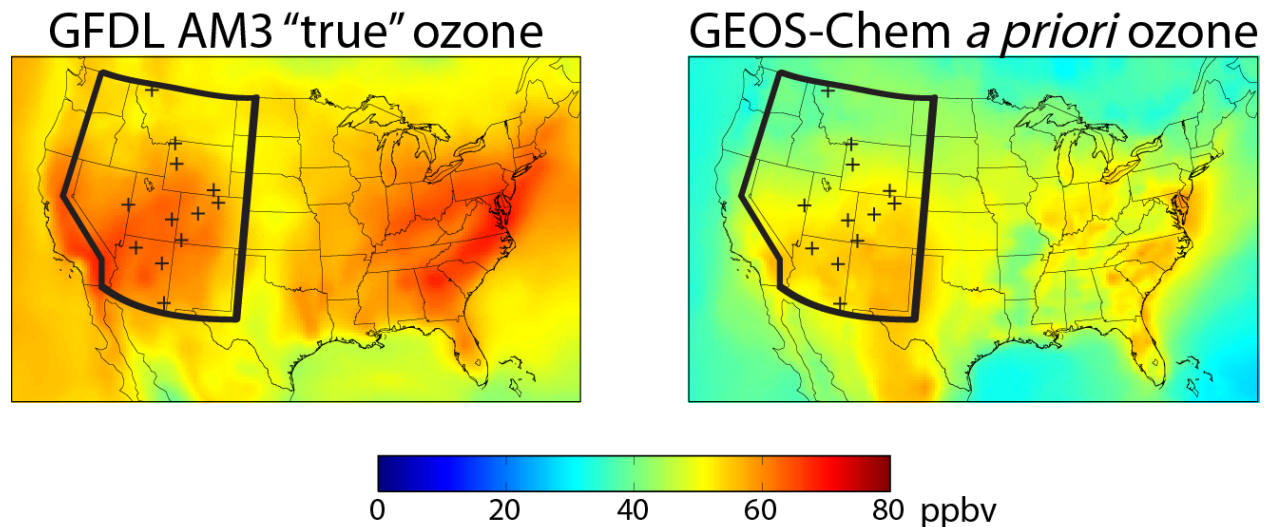
404 Use of the complete observing system described here (surface, geostationary, and LEO)
405 will provide a powerful tool for future air quality policy. Planning is underway to combine this
406 system with regional air quality models to supply the public with near real time pollution reports
407 and forecasts. These reports and forecasts would be much the same as currently available
408 weather information, also provided in large part from geostationary satellite observations.

409

410 **Acknowledgements:** This work was supported by the NASA Earth Science Division and by a NASA
411 Earth and Space Science Fellowship to Peter Zoogman.

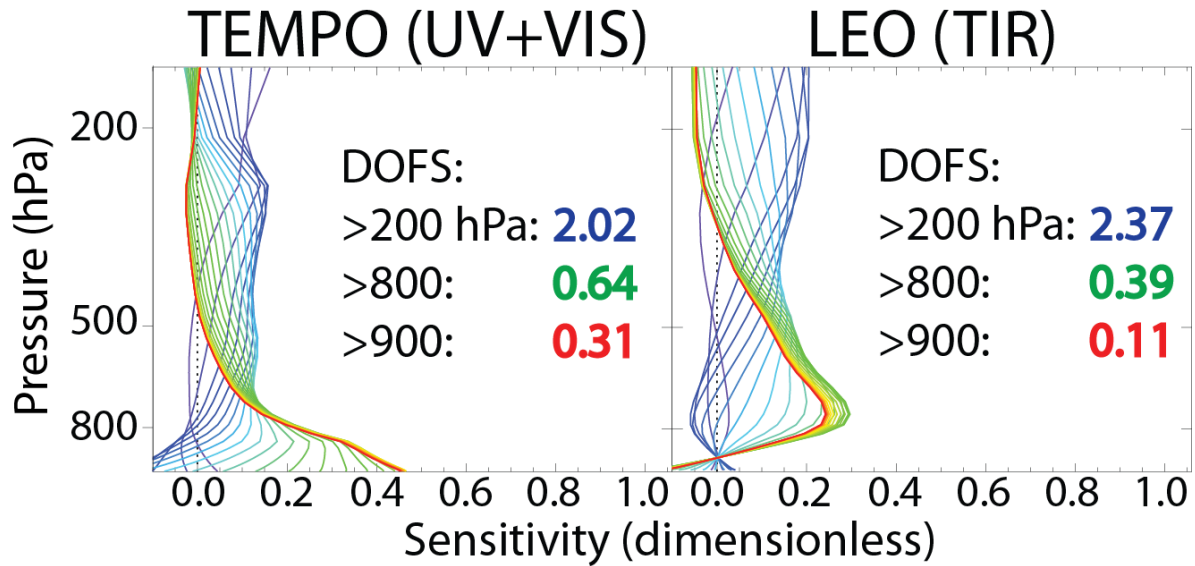
412

413 **Figures:**



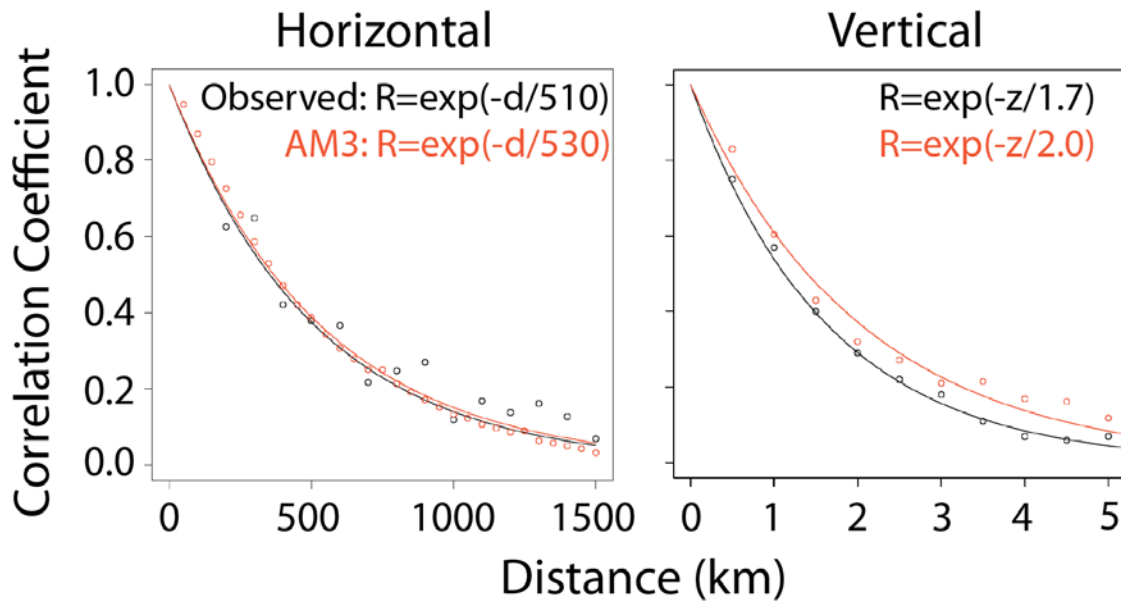
414

415 **Figure 1:** Mean values of the daily maximum 8-hour average (MDA8) ozone concentrations for
416 April-June 2010 in surface air. Left panel shows values from the GFDL AM3 CCM used as the
417 "true" atmosphere in our OSSE. Right panel shows the *a priori* values from the GEOS-Chem
418 CTM used for data assimilation. The black lines delineate the Intermountain West and black
419 crosses show CASTNet surface measurement sites in the region.



420

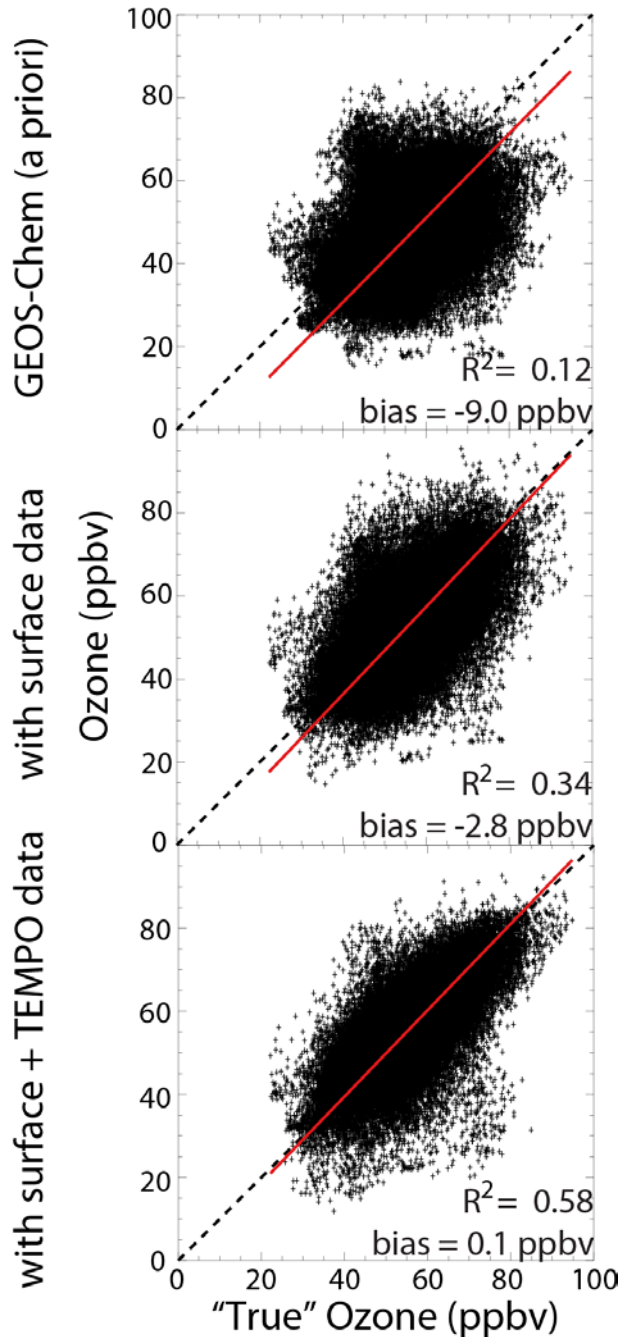
421 **Figure 2:** Normalized averaging kernel matrices assumed in this study (from Natraj et al. [2011])
 422 for clear-sky retrievals of tropospheric ozone from space in the UV+Vis (left) and the TIR
 423 (right). UV+Vis in our study corresponds to TEMPO, while TIR corresponds to a future LEO
 424 instrument flying concurrently with TEMPO. Lines are matrix rows for individual vertical levels,
 425 with the color gradient from red to blue corresponding to vertical levels ranging from surface air (red)
 426 to 200 hPa (blue). Inset are the degrees of freedom for signal (DOFS) for the atmospheric columns
 427 below 200, 800, and 900 hPa.



428

429 **Figure 3:** Error correlation length scales for the GEOS-Chem model simulation of tropospheric
 430 ozone in the US Intermountain West. The error correlations are relative to actual CASTNet and
 431 ozonesonde observations (in black) and relative to the GFDL AM3 model sampled in the
 432 Intermountain West region (in red). Statistics are computed for April-June 2010. The left panel
 433 shows the correlation coefficient (R) of the model error between pairs of CASTNet sites, plotted

434 against the distance between sites. Values are for the 12 CASTNet sites in the Intermountain
 435 West (Figure 1). The right panel shows the correlation coefficient of the model error between
 436 pairs of vertical levels (up to 8 km altitude) for ozonesonde measurements from the IONS-2010
 437 campaign in California [Cooper et al. 2011], plotted against distance between levels.
 438 Exponential fits to the data are shown inset, where d and z are horizontal and vertical distances in
 439 km.

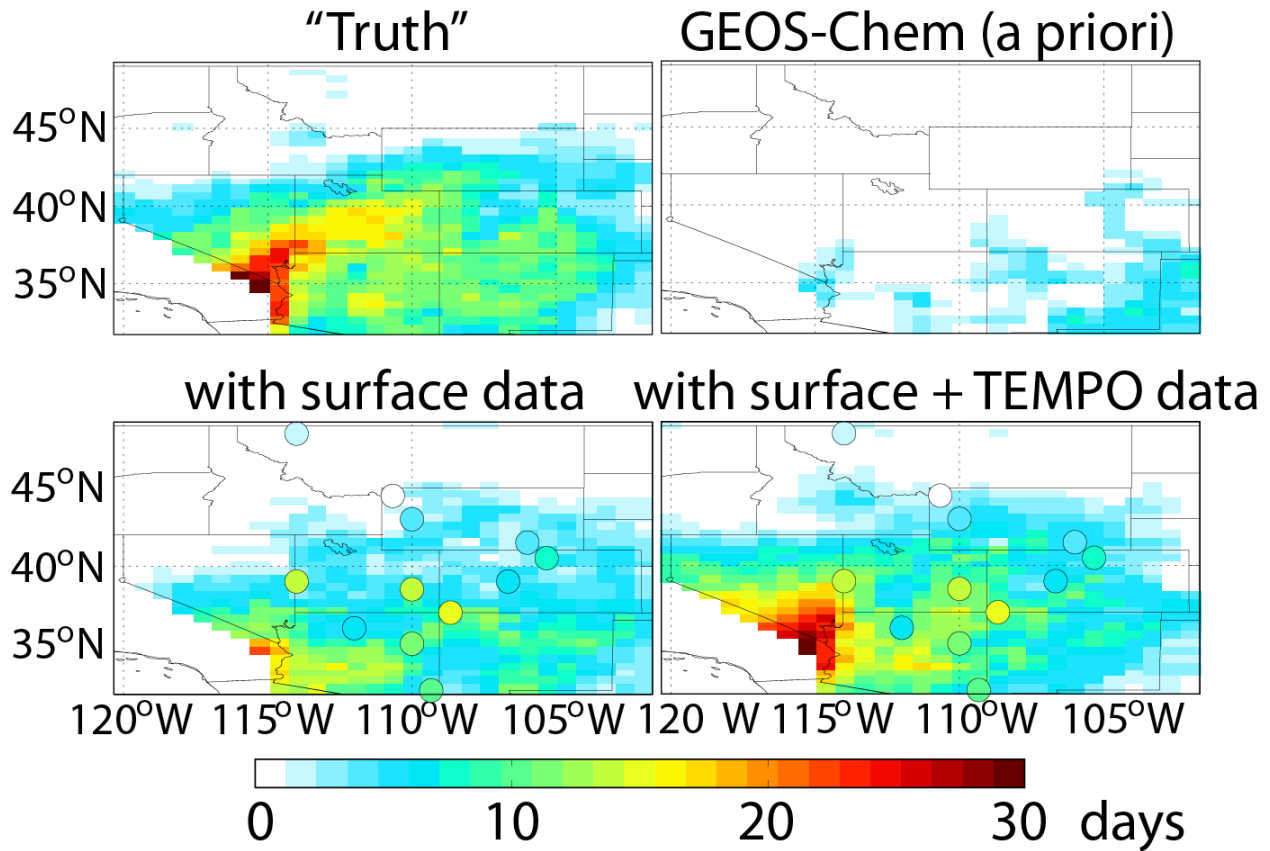


440

441 **Figure 4:** Improved monitoring of surface ozone across the Intermountain West from
 442 assimilation of synthetic CASTNet (surface) and TEMPO (geostationary satellite) observations.
 443 The figure shows scatterplots of simulated (GEOS-Chem) vs. “truth” (GFDL AM3) daily

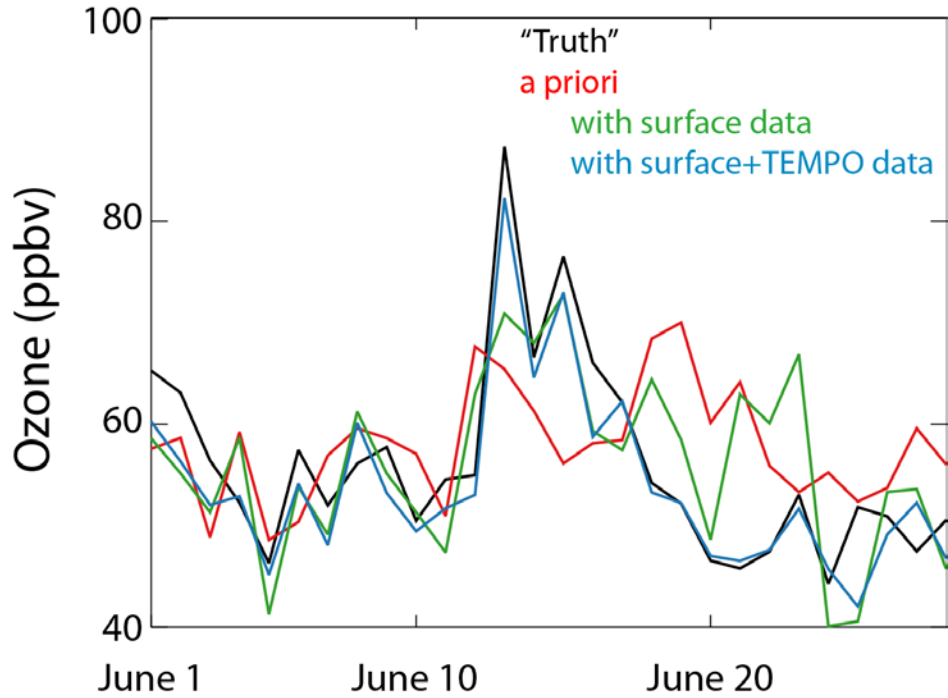
444 maximum 8-h (MDA8) surface ozone for April-June 2010 for all $1/2^\circ \times 2/3^\circ$ grid squares in the
 445 region (Figure 1) and for individual days. Results are for GEOS-Chem without data assimilation
 446 (top), with assimilation of CASTnet synthetic surface data (middle), and with additional
 447 assimilation of TEMPO and LEO synthetic satellite data (bottom). Comparison statistics are
 448 inset. Also shown are the reduced-major-axis (RMA) regression line and the 1:1 line.

Number of days with MDA8 ozone > 70 ppbv

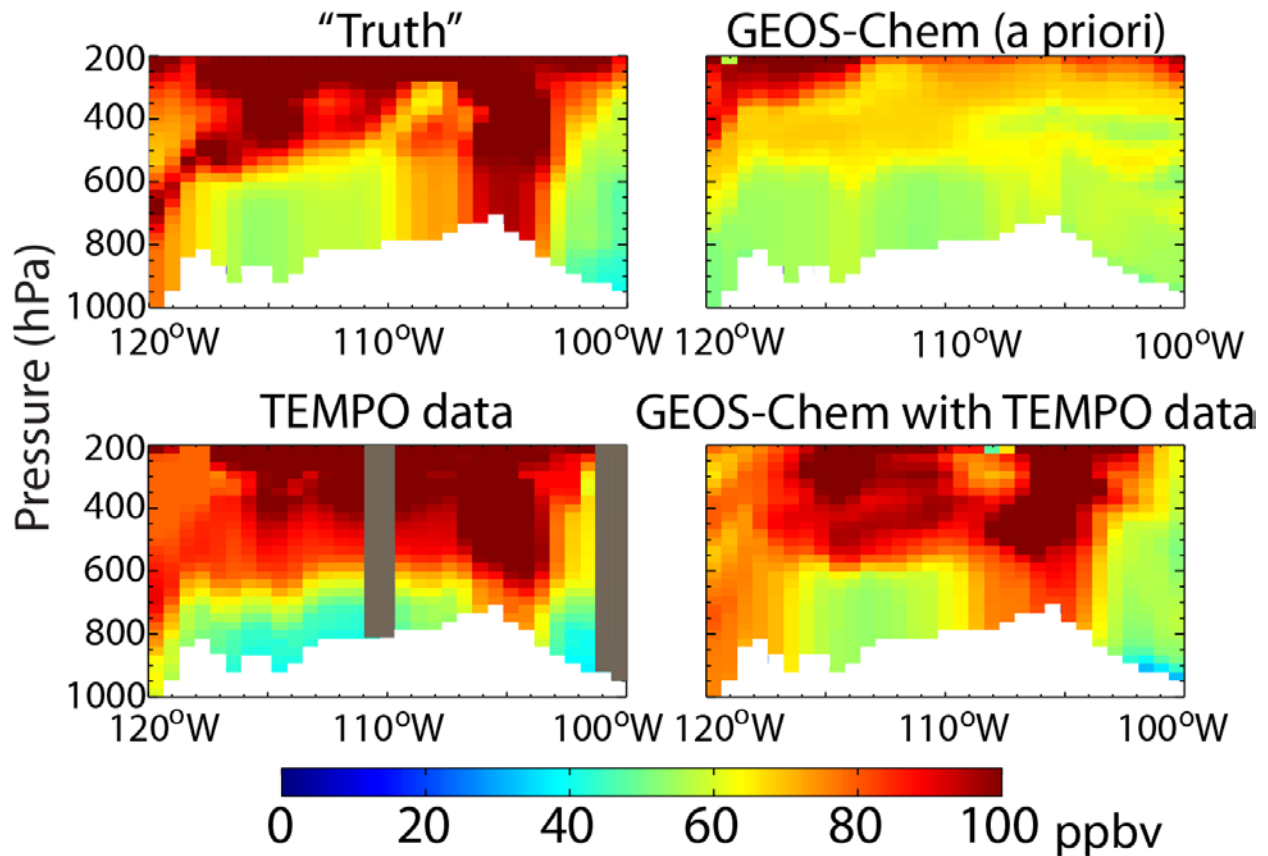


449

450 **Figure 5:** Improved detection of high-ozone events in the Intermountain West by data
 451 assimilation. The figure shows the number of events (daily maximum 8-h ozone > 70 ppbv) in
 452 April-June 2010 on the GEOS-Chem grid. The “truth” defined by the GFDL AM3 model (top
 453 left panel) is compared to GEOS-Chem simulations without data assimilation (top right), with
 454 assimilation of synthetic CASTNet surface data (bottom left), and with additional assimilation of
 455 synthetic TEMPO and LEO satellite data (bottom right). Locations of CASTNet surface sites
 456 used for assimilation with their “true” values are overlain in the bottom panels.



457
 458 **Figure 6:** Detection of an exceptional ozone event by TEMPO. The Figure shows the June 2010
 459 time series of daily maximum 8-h (MDA8) ozone concentrations at a location in northern New
 460 Mexico (107°W, 36°N) featuring a major stratospheric intrusion on June 13 in the GFDL AM3
 461 model taken as the “truth” (black line). The ability to capture this event is examined for the
 462 GEOS-Chem model without data assimilation (a priori, red line) and with assimilation of surface
 463 measurements only (green line) and satellite measurements added (blue line).



464
 465 **Figure 7:** Longitude-altitude cross-section of ozone concentrations (36°N, 2100 MT on June 13,
 466 2010) associated with the stratospheric intrusion of Figure 6. The “true” state from the GFDL
 467 AM3 model (top left) is compared to the GEOS-Chem model without data assimilation (top
 468 right) and with assimilation of surface and satellite data (bottom right). The bottom left panel
 469 shows synthetic TEMPO observations of the “true” state (gray regions indicate cloudy scenes)
 470 without data assimilation. Orange and red values indicate ozone levels that would lead to
 471 exceedances of the current National Ambient Air Quality Standard (NAAQS) of 75 ppbv. Local
 472 topography is shown in white.
 473

474 **References:**

475 Arnold, C. and Dey, C., 1986. Observing-systems simulation experiments - past, present, and
 476 future. *Bulletin of the American Meteorological Society* 67, 687-695.

477 August, T., Klaes, D., Schluessel, P., Hultberg, T., Crapeau, M., Arriaga, A., O'Carroll, A.,
 478 Coppens, D., Munro, R., Calbet, X., 2012. IASI on metop-A: Operational level 2
 479 retrievals after five years in orbit. *Journal of Quantitative Spectroscopy & Radiative*
 480 *Transfer* 113, 1340-1371.

481 Bak, J., Kim, J.H., Liu, X., Chance, K., Kim, J., 2013. Evaluation of ozone profile and
482 tropospheric ozone retrievals from GEMS and OMI spectra. *Atmospheric Measurement*
483 *Techniques* 6, 239-249.

484 Bey, I., Jacob, D., Yantosca, R., Logan, J., Field, B., Fiore, A., Li, Q., Liu, H., Mickley, L.,
485 Schultz, M., 2001. Global modeling of tropospheric chemistry with assimilated
486 meteorology: Model description and evaluation. *Journal of Geophysical Research-*
487 *Atmospheres* 106, 23073-23095.

488 Brodin, M., Helmig, D., Oltmans, S., 2010. Seasonal ozone behavior along an elevation gradient
489 in the colorado front range mountains. *Atmospheric Environment* 44, 5305-5315.

490 Chance, K., Lui, X., Suleiman, R.M., Flittner, D.E., Janz, S.J., 2012. Tropospheric Emissions:
491 Monitoring of Pollution (TEMPO). Abstract A31B-0020 presented at the 2012 AGU Fall
492 Meeting.

493 Chance, K., Burrows, J., Perner, D., Schneider, W., 1997. Satellite measurements of atmospheric
494 ozone profiles, including tropospheric ozone, from ultraviolet/visible measurements in
495 the nadir geometry: A potential method to retrieve tropospheric ozone. *Journal of*
496 *Quantitative Spectroscopy & Radiative Transfer* 57, 467-476.

497 Claeysman, M., Attie, J-L., Peuch, V-H., El Amraoui, L., Lahoz, W.A., Josse, B., Joly, M., Barre,
498 J., Ricaud, P., Massart, S., Piacentini, A., von Clarmann, T., Hopfner, M., Orphal, J.,
499 Flaud, J.M., Edwards, D.P., 2011. A thermal infrared instrument onboard a geostationary
500 platform for CO and O-3 measurements in the lowermost troposphere: Observing System
501 Simulation Experiments (OSSE). *Atm. Meas. Tech.*, 4, 1637-1661.

502 Clerbaux, C., Boynard, A., Clarisse, L., George, M., Hadji-Lazaro, J., Herbin, H., Hurtmans, D.,
503 Pommier, M., Razavi, A., Turquety, S., Wespes, C., Coheur, P.-., 2009. Monitoring of
504 atmospheric composition using the thermal infrared IASI/MetOp sounder. *Atmospheric*
505 *Chemistry and Physics* 9, 6041-6054.

506 Cooper, O.R., Oltmans, S.J., Johnson, B.J., Brioude, J., Angevine, W., Trainer, M., Parrish,
507 D.D., Ryerson, T.R., Pollack, I., Cullis, P.D., Ives, M.A., Tarasick, D.W., Al-Saadi, J.,
508 Stajner, I., 2011. Measurement of western US baseline ozone from the surface to the
509 tropopause and assessment of downwind impact regions. *Journal of Geophysical*
510 *Research-Atmospheres* 116, D00V03.

511 Cooper, O.R., Gao, R., Tarasick, D., Leblanc, T., Sweeney, C., 2012. Long-term ozone trends at
512 rural ozone monitoring sites across the United States, 1990-2010. *Journal of Geophysical*
513 *Research-Atmospheres* 117, D22307.

514 Edwards, D.P., Arellano, A.F., Jr., Deeter, M.N., 2009. A satellite observation system simulation
515 experiment for carbon monoxide in the lowermost troposphere. *Journal of Geophysical*
516 *Research-Atmospheres* 114, D14304.

- 517 Emery, C., Jung, J., Downey, N., Johnson, J., Jimenez, M., Yarvwood, G., Morris, R., 2012.
518 Regional and global modeling estimates of policy relevant background ozone over the
519 United States. *Atmospheric Environment* 47, 206-217.
- 520 Fiore, A., Jacob, D., Liu, H., Yantosca, R., Fairlie, T., Li, Q., 2003. Variability in surface ozone
521 background over the United States: Implications for air quality policy. *Journal of*
522 *Geophysical Research-Atmospheres* 108, 4787.
- 523 Fiore, A., Jacob, D., Bey, I., Yantosca, R., Field, B., Fusco, A., Wilkinson, J., 2002. Background
524 ozone over the United States in summer: Origin, trend, and contribution to pollution
525 episodes. *Journal of Geophysical Research-Atmospheres* 107, 4275.
- 526 Fishman, J., Iraci, L.T., Al-Saadi, J., Chance, K., Chavez, F., Chin, M., Coble, P., Davis, C.,
527 DiGiacomo, P.M., Edwards, D., Eldering, A., Goes, J., Herman, J., Hu, C., Jacob, D.J.,
528 Jordan, C., Kawa, S.R., Key, R., Liu, X., Lohrenz, S., Mannino, A., Natraj, V., Neil, D.,
529 Neu, J., Newchurch, M., Pickering, K., Salisbury, J., Sosik, H., Subramaniam, A.,
530 Tzortziou, M., Wang, J., Wang, M., 2012. The united states' next generation of
531 atmospheric composition and coastal ecosystem measurements NASA's geostationary
532 coastal and air pollution events (GEO-CAPE) mission. *Bulletin of the American*
533 *Meteorological Society* 93, 1547-+.
- 534 Fu, D., Worden, J.R., Liu, X., Kulawik, S.S., Bowman, K.W., Natraj, V., 2013. Characterization
535 of ozone profiles derived from aura TES and OMI radiances. *Atmospheric Chemistry and*
536 *Physics* 13, 3445-3462.
- 537 Ingmann, P., Veihelmann, B., Langen, J., Lamarre, D., Stark, H., Courreges-Lacoste, G.B., 2012.
538 Requirements for the GMES atmosphere service and ESA's implementation concept:
539 Sentinels-4/-5 and-5p. *Remote Sensing of Environment* 120, 58-69.
- 540 Jaffe, D., 2011. Relationship between surface and free tropospheric ozone in the western U.S.
541 *Environmental science & technology* 45, 432-438.
- 542 Jaffe, D.A. and Wigder, N.L., 2012. Ozone production from wildfires: A critical review.
543 *Atmospheric Environment* 51, 1-10.
- 544 Kaynak, B., Hu, Y., Martin, R.V., Russell, A.G., Choi, Y., Wang, Y., 2008. The effect of
545 lightning NO_x production on surface ozone in the continental united states. *Atmospheric*
546 *Chemistry and Physics* 8, 5151-5159.
- 547 Khattatov, B., Lamarque, J., Lyjak, L., Menard, R., Levelt, P., Tie, X., Brasseur, G., Gille, J.,
548 2000. Assimilation of satellite observations of long-lived chemical species in global
549 chemistry transport models. *Journal of Geophysical Research-Atmospheres* 105, 29135-
550 29144.

- 551 Kim, J., 2012. GEMS (Geostationary Environment Monitoring Spectrometer) onboard the
552 GeoKOMPSAT to monitor air quality in high temporal and spatial resolution over Asia-
553 Pacific region. Abstract EGU2012-4051 presented at the 2012 EGU General Assembly.
- 554 Lahoz, W.A., Peuch, V.-H., Orphal, J., Attie, J.-L., Chance, K., Liu, X., Edwards, D., Elbern, H.,
555 Flaud, J.-M., Claeys, M., El Amraoui, L., 2012. Monitoring air quality from space: the
556 case for the geostationary platform. *Bulletin of the American Meteorological Society* 11,
557 221-233.
- 558 Langford, A.O., Aikin, K.C., Eubank, C.S., Williams, E.J., 2009. Stratospheric contribution to
559 high surface ozone in Colorado during springtime. *Geophysical Research Letters* 36,
560 L12801.
- 561 Lefohn, A., Oltmans, S., Dann, T., Singh, H., 2001. Present-day variability of background ozone
562 in the lower troposphere. *Journal of Geophysical Research-Atmospheres* 106, 9945-9958.
- 563 Lin, M., Fiore, A.M., Cooper, O.R., Horowitz, L.W., Langford, A.O., Levy, Hiram, II, Johnson,
564 B.J., Naik, V., Oltmans, S.J., Senff, C.J., 2012. Springtime high surface ozone events
565 over the western United States: Quantifying the role of stratospheric intrusions. *Journal*
566 *of Geophysical Research-Atmospheres* 117, D00V22.
- 567 Lin, M., Fiore, A.M., Horowitz, L.W., Cooper, O.R., Naik, V., Holloway, J., Johnson, B.J.,
568 Middlebrook, A.M., Oltmans, S.J., Pollack, I.B., Ryerson, T.B., Warner, J.X.,
569 Wiedinmyer, C., Wilson, J., Wyman, B., 2012. Transport of asian ozone pollution into
570 surface air over the western United States in spring. *Journal of Geophysical Research-*
571 *Atmospheres* 117, D00V07.
- 572 Liu, X., Sioris, C., Chance, K., Kurosu, T., Newchurch, M., Martin, R., Palmer, P., 2005.
573 Mapping tropospheric ozone profiles from an airborne ultraviolet-visible spectrometer.
574 *Applied Optics* 44, 3312-3319.
- 575 Lord, S.J., Kalnay E., Daley R., Emmitt G.D., Atlas R., 1997. Using OSSEs in the design of future g
576 eneration integrated observing systems. Preprints, 1st Symposium on Integrated Observing
577 Systems, Long Beach, CA, AMS, 45-47.
- 578 Mueller, S.F. and Mallard, J.W., 2011. Contributions of natural emissions to ozone and PM_{2.5} as
579 simulated by the community multiscale air quality (CMAQ) model. *Environmental*
580 *science & technology* 45, 4817-4823.
- 581 Natraj, V., Liu, X., Kulawik, S., Chance, K., Chatfield, R., Edwards, D.P., Eldering, A., Francis,
582 G., Kurosu, T., Pickering, K., Spurr, R., Worden, H., 2011. Multi-spectral sensitivity
583 studies for the retrieval of tropospheric and lowermost tropospheric ozone from simulated
584 clear-sky GEO-CAPE measurements. *Atmospheric Environment* 45, 7151-7165.
- 585 Parrington, M., Jones, D.B.A., Bowman, K.W., Horowitz, L.W., Thompson, A.M., Tarasick,
586 D.W., Witte, J.C., 2008. Estimating the summertime tropospheric ozone distribution over

587 North America through assimilation of observations from the tropospheric emission
588 spectrometer. *Journal of Geophysical Research-Atmospheres* 113, D18307.

589 Parrish, D.D., Aiken, K.C., Oltmans, S.J., Johnson, B.J., Ives, M., Sweeny, C., 2010. Impact of
590 transported background ozone inflow on summertime air quality in a California ozone
591 exceedances area. *Atmospheric Chemistry and Physics* 10, 10093-10109.

592 Reid, N., Yap, D., Bloxam, R., 2008. The potential role of background ozone on current and
593 emerging air issues: An overview. *Air Quality Atmosphere and Health* 1, 19-29.

594 Rodgers, C.D., 2000. *Inverse Methods for Atmospheric Sounding*. World Scientific, River Edge,
595 New Jersey.

596 Selitto, P., Dufour, G., Eremenko, M., Cuesta, J., Foret, G., Gaubert, B., Beekmann, M., Peuch,
597 V.-H., Flaud, J.-M., 2014. Monitoring the lowermost tropospheric ozone with thermal
598 infrared observations from a geostationary platform: performance analyses for a future
599 dedicated instrument. *Atmospheric Measurement Techniques* 7, 391-407.

600 Selitto, P., Del Frate, F., Solimini, D., Casadio, S., 2012. Tropospheric ozone column retrieval
601 from ESA-Envisat SCIAMACHY nadir UV/VIS radiance measurements by means of a
602 neural network algorithm. *IEEE Transactions on Geosciences and Remote Sensing* 50,
603 998-1011.

604 Selitto, P., Di Noia, A., Del Frate, F., Burini, A., Casadio, S., Solimini, D., 2012. On the role of
605 visible radiation in ozone profile retrieval from nadir UV/VIS satellite measurements: An
606 experiment with neural network algorithms inverting SCIAMACHY data. *Journal of*
607 *Quantitative Spectroscopy and Radiative Transfer* 113, 1429-1436.

608 Singh, H.B., Cai, C., Kaduwela, A., Weinheimer, A., Wisthaler, A., 2012. Interactions of fire
609 emissions and urban pollution over California: Ozone formation and air quality
610 simulations. *Atmospheric Environment* 56, 45-51.

611 Timmermans, R.M.A., Segers, A.J., Builtjes, P., Vautard, R., Siddans, R., Elbern, H., Tjemkes,
612 S., Schaap, M., 2009. The added value of a proposed satellite imager for ground level
613 particulate matter analyses and forecasts. *IEEE J. Sel. Top. Appl.*, 2, 271-283.

614 United States Environmental Protection Agency, 2010. Clean air status and trends network
615 second quarter 2010 quality assurance report.

616 United States Environmental Protection Agency, 2012. *Welfare Risk and Exposure Assessment*
617 *for Ozone*.

618 United States Environmental Protection Agency, 2013. *Interim Guidance to Implement*
619 *Requirements for the Treatment of Air Quality Monitoring Data Influenced by*
620 *Exceptional Events*.

- 621 Worden, H.M., Deeter, M.N., Frankenberg, C., George, M., Nichitiu, F., Worden, J., Aben, I.,
622 Bowman, K.W., Clerbaux, C., Coheur, P.F., de Laat, A.T.J., Detweiler, R., Drummond,
623 J.R., Edwards, D.P., Gille, J.C., Hurtmans, D., Luo, M., Martinez-Alonso, S., Massie, S.,
624 Pfister, G., Warner, J.X., 2013. Decadal record of satellite carbon monoxide observations.
625 *Atmospheric Chemistry and Physics* 13, 837-850.
- 626 Yates, E.L., Iraci, L.T., Pierce, R.B., Johnson, M.S., Reddy, P.J., Tadic, J.M., Loewenstein, M.,
627 Gore, W., 2013. Airborne observations and modeling of springtime stratosphere-to-
628 troposphere transport over California. *Atmos. Chem. Phys. Discuss.* 13,
- 629 Zhang, L., Jacob, D.J., Boersma, K.F., Jaffe, D.A., Olson, J.R., Bowman, K.W., Worden, J.R.,
630 Thompson, A.M., Avery, M.A., Cohen, R.C., Dibb, J.E., Flock, F.M., Fuelberg, H.E.,
631 Huey, L.G., McMillan, W.W., Singh, H.B., Weinheimer, A.J., 2008. Transpacific
632 transport of ozone pollution and the effect of recent Asian emission increases on air
633 quality in North America: An integrated analysis using satellite, aircraft, ozonesonde, and
634 surface observations. *Atmospheric Chemistry and Physics* 8, 6117-6136.
- 635 Zhang, L., Jacob, D.J., Liu, X., Logan, J.A., Chance, K., Eldering, A., Bojkov, B.R., 2010.
636 Intercomparison methods for satellite measurements of atmospheric composition:
637 Application to tropospheric ozone from TES and OMI. *Atmospheric Chemistry and*
638 *Physics* 10, 4725-4739.
- 639 Zhang, L., Jacob, D.J., Downey, N.V., Wood, D.A., Blewitt, D., Carouge, C.C., van Donkelaar,
640 A., Jones, D.B.A., Murray, L.T., Wang, Y., 2011. Improved estimate of the policy-
641 relevant background ozone in the United States using the GEOS-chem global model with
642 1/2 degrees x 2/3 degrees horizontal resolution over North America. *Atmospheric*
643 *Environment* 45, 6769-6776.
- 644 Zoogman, P., Jacob, D.J., Chance, K., Worden, H.M., Edwards, D.P., Zhang, L., 2014. Improved
645 monitoring of surface ozone air quality by joint assimilation of geostationary satellite
646 observations of ozone and CO. *Atmospheric Environment* 84, 254-261.
- 647 Zoogman, P., Jacob, D.J., Chance, K., Zhang, L., Le Sager, P., Fiore, A.M., Eldering, A., Liu,
648 X., Natraj, V., Kulawik, S.S., 2011. Ozone air quality measurement requirements for a
649 geostationary satellite mission. *Atmospheric Environment* 45, 7143-7150.